Acta Biomaterialia 7 (2011) 3094–3100

Contents lists available at ScienceDirect

Acta Biomaterialia

journal homepage: www.elsevier.com/locate/actabiomat

Synthesis of a novel photopolymerized nanocomposite hydrogel for treatment of acute mechanical damage to cartilage

Kathryn E. Schlichting [a], Trishelle M. Copeland-Johnson [b], Matthew Goodman [a], Robert J. Lipert [c], Tanya Prozorov [f], Xunpei Liu [e], Todd O. McKinley [d], Zhiqun Lin [a], James A. Martin [d], Surya K. Mallapragada [a,e,f,*]

[a] Department of Materials Science and Engineering, Iowa State University, USA
[b] Department of Chemical Engineering, University of South Florida, USA
[c] Institute for Combinatorial Discovery, Iowa State University, USA
[d] Department of Orthopaedic Surgery and Rehabilitation, University of Iowa, Ames, IA 50011, USA
[e] Department of Chemical and Biological Engineering, Iowa State University, USA
[f] Division of Materials Sciences and Engineering, Ames Laboratory, USA

ARTICLE INFO

Article history:
Received 30 December 2010
Received in revised form 4 April 2011
Accepted 14 April 2011
Available online 20 April 2011

Keywords:
Nanocomposite
Hydrogel
Biomaterials
Injectable
Cartilage

ABSTRACT

Intra-articular fractures initiate a cascade of pathobiological and pathomechanical events that culminate in post-traumatic osteoarthritis (PTOA). Hallmark features of PTOA include destruction of the cartilage matrix in combination with loss of chondrocytes and acute mechanical damage (AMD). Currently, treatment of intra-articular fractures essentially focuses completely on restoration of the macroanatomy of the joint. However, current treatment ignores AMD sustained by cartilage at the time of injury. We are exploring aggressive biomaterial-based interventions designed to treat the primary pathological components of AMD. This study describes the development of a novel injectable co-polymer solution that forms a gel at physiological temperatures that can be photocrosslinked, and can form a nanocomposite gel in situ through mineralization. The injectable co-polymer solution will allow the material to fill cracks in the cartilage after trauma. The mechanical properties of the nanocomposite are similar to those of native cartilage, as measured by compressive and shear testing. It thereby has the potential to mechanically stabilize and restore local structural integrity to acutely injured cartilage. Additionally, in situ mineralization ensures good adhesion between the biomaterial and cartilage at the interface, as measured through tensile and shear testing. Thus we have successfully developed a new injectable co-polymer which forms a nanocomposite in situ with mechanical properties similar to those of native cartilage, and which can bond well to native cartilage. This material has the potential to stabilize injured cartilage and prevent PTOA.
© 2011 Acta Materialia Inc. Published by Elsevier Ltd. All rights reserved.

1. Introduction

Intra-articular fractures initiate a cascade of pathobiological and pathomechanical events that culminate in post-traumatic osteoarthritis (PTOA) [1–5]. Hallmark features of PTOA include destruction of the cartilage matrix in combination with loss of chondrocytes [6–12]. The etiology of PTOA is multifactorial, but a major pathoetiologic component hypothesized to incite and propagate this destructive cascade is acute mechanical damage (AMD) sustained by the cartilage at the time of injury [12–15]. AMD affects the structural integrity of the cartilage and causes chondrocyte metabolic dysfunction and death [7,14,16–18]. Chondrocytes subjected to pathological strains become increasingly metabolically incompetent or die, and no longer produce effective matrix molecules. This, in turn, leads to further matrix damage and further chondrocyte death. This relationship becomes self-propagating, and has been hypothesized to cause PTOA.

Currently, treatment of intra-articular fractures focuses completely on restoration of the macroanatomy of the joint [3,19,20]. The treatment premise is that restoring the macroanatomy of the joint will prevent ongoing pathomechanical stresses and this will in turn prevent cartilage degeneration. Articular fragments are reduced and metaphyseal disruptions are realigned to restore the congruity, stability, and alignment of the injured joint. However, current treatment ignores AMD sustained by cartilage at the time of injury. Furthermore, the outcomes of intra-articular fractures treated using even the most sophisticated techniques have not improved appreciably in decades (Fig. 1). Taken together, the next significant improvement in outcomes of intra-articular fractures will likely involve developing effective treatment measures aimed at mitigating AMD.

* Corresponding author at: Department of Chemical and Biological Engineering, Iowa State University, USA. Tel.: +1 515 294 7407; fax: +1 515 294 2689.
E-mail address: suryakm@iastate.edu (S.K. Mallapragada).

1742-7061/$ - see front matter © 2011 Acta Materialia Inc. Published by Elsevier Ltd. All rights reserved.
doi:10.1016/j.actbio.2011.04.010

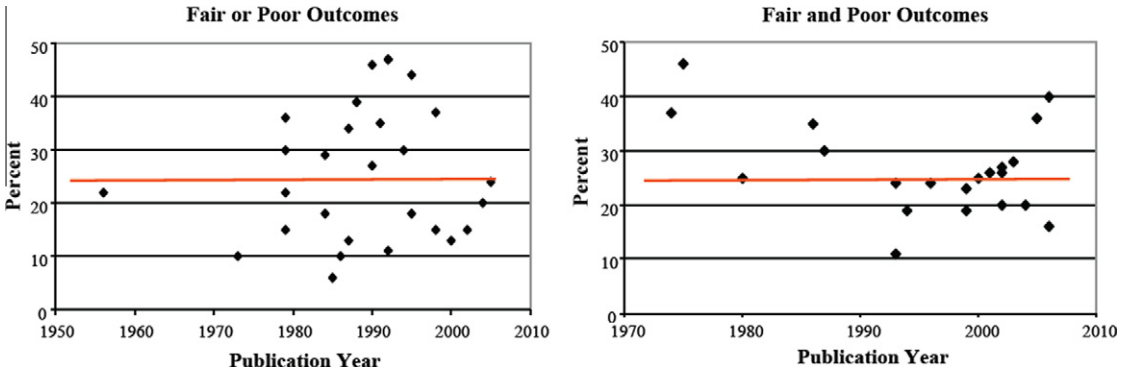

Fig. 1. Fair and poor outcomes for tibial plateau fractures (left) and acetabular fractures (right). Results have seen no improvement for decades.

We propose that a new paradigm in treating intra-articular fractures is necessary to improve outcomes. We have hypothesized that restoration of native mechanical properties to impact-injured cartilage can reduce chondrocyte death and improve chondrocyte metabolic dysfunction after an impact injury. The premise is that in the acute and subacute period after an intra-articular fracture there is a continuum of injury among chondrocytes in the region of AMD. Within this continuum of injury there is a population of chondrocytes that are injured but have the potential to heal and become metabolically productive if they receive appropriate treatment. We propose that impact-injured chondrocytes have the potential to heal if they are protected from ongoing AMD-related hazardous strains. Furthermore, injured chondrocytes could also be nurtured by local delivery of therapeutic chondrocyte-enhancing bioactive agents. Maximizing the number of metabolically competent chondrocytes in regions of AMD has the potential to mitigate or arrest the self-propagating cascade leading to PTOA.

We conceived that a material that could penetrate the interstitium of damaged cartilage, bond with the surrounding cartilage, and restore local material properties could shield injured chondrocytes from ongoing injury-related hazardous strains which could determine whether an injured chondrocyte proceeds to cell death or recovers and becomes biologically productive. Furthermore, such a material could also deliver chondrocyte-enhancing bioactive agents to locally injured chondrocytes. The strategy is simple: deliver mechanical and biological treatment preferentially to regions of AMD (matrix cracks and fracture edges). However, it requires the development of a biomaterial that can fill cracks in the cartilage and exhibit mechanical properties similar to those of native cartilage and good binding with the cartilage. This study describes the development of such an injectable nanocomposite photopolymerizing copolymer that has the potential to restore local structural integrity to acutely injured cartilage, and subsequently act as a carrier for chondrocyte-enhancing bioactive agents. This material design is based on our earlier work on the development of novel injectable nanocomposites formed by self-assembling polymers with attached mineralization peptides acting as templates for the nucleation and growth of inorganic nanocrystals [21–23]. In this investigation we have designed this material to be formulated as a liquid which can be photopolymerized to a solid and can develop material properties that are of the same magnitude as native cartilage. In this study we describe the synthesis of the material and optimization of the material properties to meet our requirements as listed above.

2. Materials and methods

2.1. Materials

Specific materials used in this project include PEG-1000 [poly(ethylene glycol) 1000 dimethacrylate] (Fp 220°F, specific gravity 1.1) synthesized by Polysciences Inc. (Warrington, PA). The Pluronic F-127 co-polymer (poly(ethylene oxide)-*b*-poly(propylene oxide)-*b*-poly(ethylene oxide)) (MW_n 12,600 Da) was a product of BASF Corp. (Florham Park, NJ). N-hydroxysuccinimide (NHS) (MW 115.09 g mol^{-1}, ⩾97% purity) and succinic anhydride (MW 100.1) were obtained from Sigma–Aldrich (St. Louis, MO). The collagen binding peptide (CBP) (GLRSKSKKFRRPDIQYPDATDED...) (97.9% purity, MW 3292.71) and hydroxyapatite binding peptide (HBP) (DSKSDSSKSESDSS) (~95% purity, MW 1445 Da) were synthesized by Genscript Corp. (Piscataway, NJ). Pyridine (MW 79.1, certified ACS grade), anhydrous diethyl ether (MW 74.1), toluene (MW 92.1, certified ACS grade), and dichloromethane (MW 84.9, pesticide grade) were purchased from Fisher Scientific (Hanover Park, IL). *N*,*N*-Dicyclohexylcarbodiimide (MW 206.3) was from Avocado Research Chemicals (Morecombe, UK). The photoinitiator for assistance in crosslinked hydrogel formation was Igracure® 2959 (4-(2-hydroxyethoxy) phenyl-(2-hydroxy-2-propyl) ketone) (MW 224 g mol^{-1}) synthesized by Ciba AG (Basel, Switzerland). Cartilage samples were obtained from bovine patellae obtained from a local slaughterhouse. The patellae were kept frozen and then thawed at room temperature prior to sample preparation. The Omnicure Series 1000 IB UV radiation lamp used for photocrosslinking was manufactured by EXFO Photonic Solutions Inc. (Quebec, Canada).

2.2. Nanocomposite synthesis

The hydroxyl end groups of Pluronic F-127 were converted to carboxyl groups by treatment with succinic anhydride in pyridine as reported in the literature [24]. Pluronic F-127 (32 g, 2.5 mmol) and succinic anhydride (1 g, 10 mmol) were dissolved in pyridine (100 ml), and the reaction carried out at 40 °C for 24 h. The mixture was then precipitated in diethyl ether, dissolved in toluene, and reprecipitated in diethyl ether. The product was then dried under vacuum. The carboxyl terminated Pluronic F-127 was esterified with NHS as reported in the literature [25]. Pluronic F-127 (0.128 mmol), 0.0792 g of *N*,*N*-dicyclohexylcarbodiimide (3 × excess, 0.384 mol), 0.0442 g of NHS (3 × excess, 0.384 mol), and 8 ml of dichloromethane were added to a round-bottomed flask connected with an argon line and bubbler. The reaction was carried out at room temperature for 24 h. The reaction mixture was then filtered and precipitated in cold diethyl ether. NHS attachment was verified by 1H NMR with ester peak at approximately 2.7 ppm and was found to be around 1% (w/v). The NHS-functionalized polymer was then conjugated with HBP and/or CBP peptide. NHS polymer (1.5 g) was added to a solution of 12 mg of peptide in 50 ml of phosphate-buffered saline (PBS), pH 7.4, with stirring at room temperature. After 4 h an additional 1.5 g of NHS-functionalized polymer was added to the mixture. The reaction was maintained at room temperature for 24 h. The

reaction mixture was dialyzed against water using a cellulose ester membrane with a molecular weight cut-off of 3500 (Spectrum Labs, Rancho Dominguez, CA) for 48 h to remove the uncoupled peptide. The polymer–peptide solution was then lyophilized, giving a pure white powder, and peptide attachment was then qualitatively characterized by ^{1}H NMR.

The nanocomposite gels were synthesized by following a general procedure, as shown in Fig. 2. First 90 mg of PEG-1000, followed by either 30 mg of Pluronic F-127 attached to either CBP or HBP or 15 mg each of Pluronic F-127 attached to CBP and HBP, were added to 20 ml scintillation vials. Afterwards, 250 μl of a 4 M Ca^{2+} ($CaCl_2{\cdot}2H_2O$) solution, mixed with 104 mg of the Igracure photoinitiator, was added. The vials were then refrigerated for 24 h. After that time the contents of each vial were stirred on a vortex machine to achieve a homogeneous composition, and 150 μl of a 4 M PO_4^{3-} ($(NH_4)_2HPO_4$) solution was added, to promote the nucleation and growth of calcium phosphate nanocrystals. Non-mineralized gel-forming solutions used to produce control samples were generated by replacing both the Ca^{2+} and PO_4^{3-} solutions with 400 μl of deionized water containing dissolved photoinitiator. All vials were returned to refrigeration for another 24 h.

Nanocomposite samples were then produced by photocrosslinking uniform amounts of these polymer solutions in ½ inch 10 mm outer diameter glass tubes placed in a Petri dish under a UV lamp for 120 s at 50 mW cm^{-2}. A selected group of both mineralized and non-mineralized hydrogels were generated by depositing the gel-forming solutions on bovine cartilage disks placed at the bottom of the glass tubes. Synthesized hydrogels were then allowed to swell in PBS, pH 7.2 (0.1 M Na_3PO_4 and 0.15 M NaCl). Samples were then characterized and tested after aging for 24 and 48 h.

The crystal structure of the nanocomposite was investigated by X-ray diffraction (XRD) (X'Pert PRO, PANalytical Inc., Westborough, MA). The diffractometer was operated at 45 kV and 40 mA. CuK_α radiation with a wavelength of 0.15418 nm was employed. The scan rate was 0.021°s^{-1} with a step size of 0.017° over the range $10° \leqslant 2\theta \leqslant 80°$.

The percentage of inorganic material in the nanocomposite was determined by thermogravimetric analysis (TGA 7, Perkin–Elmer). Approximately 15 mg of the hydrogel nanocomposite sample was placed in a platinum pan and heated from 20 to 700 °C at a rate of 10 °C min^{-1} under 20 ml min^{-1} nitrogen flow conditions.

Transmission electron microscopy (TEM) analysis was performed with the Tecnai G^2 F20 scanning transmission electron microscope (FEI Co., Hillsboro OR) equipped with high angle annular dark field (HAADF) and energy dispersive X-ray spectroscopy (EDS) detectors at an operating voltage of 200 keV.

The ground photocrosslinked solid specimen (20 μg) were dispersed in 5 ml of ddH_2O and left in the liquid for 24 h to ensure removal of the organic matrix. ddH_2O (2 ml) was then added to 100 μl of the suspension prepared in this manner. Diluted specimen suspension (20 μl) was deposited on a carbon-supported Quantifoil copper grid. To determine the average size of the particles in the nanocomposite multiple areas of each specimen were examined. Imaging of the nanocomposite specimens was performed without staining in bright field (BF) TEM mode.

2.3. Mechanical testing

2.3.1. Compressive modulus testing

The static compressive modulus of elasticity was determined for five samples using a dynamic mechanical analyzer (DMA 7, Perkin–Elmer). 5-mm diameter disks of the materials between 1 and 2 mm in height were used. A 0–2000 mN compressive force was applied at 30 mN min^{-1}. The five separate specimens were synthesized with photocrosslinking times ranging between 120 and 1000 s and intensities of photocrosslinking energy ranging between 20 and 50 mW. Two bovine cartilage specimens were tested as control samples.

2.3.2. Shear testing

Shear testing was conducted using an ARES RFS rheometer manufactured by TA Instruments (New Castle, DE), utilizing an 8 mm stainless steel parallel plate geometry combined with a coquette bob fixture to submerge the samples in PBS during testing. Samples were subjected to dynamic strain sweep (DSS) testing. All tests were conducted at room temperature, at a frequency of 63 rad s^{-1}, with the strain varying from 1% to 70% in increments of 1% using a linear sweep mode. Four experimental samples were tested. The first two experimental specimens were fully mineralized samples either with or without CBP added to the hydrogel. The second two experimental specimens were composite structures fabricated by bonding fully mineralized samples of the hydrogel to bovine patellofemoral cartilage. These composite hydrogel–cartilage samples were tested to determine how effectively the material bonded to cartilage. Shear tests of composite samples quantified how the composite material–cartilage structure resisted shearing load and where shearing deformation occurred. Non-mineralized variations of the hydrogel samples with or without CBP were also tested to determine the effect of mineralization. Bovine patellofemoral cartilage served as the control tissue.

2.3.3. Tensile testing

To determine how well the hydrogel enhanced with CBP bonded with cartilage tensile testing was performed on the fully mineralized hydrogel sample loaded with CBP and bonded to bovine cartilage. For this the fully mineralized samples containing CBP deposited on bovine cartilage were attached to the disc sample holder of a dynamic mechanical analyzer using superglue. The sample was then lowered until contact was made with the lower plate and attached. Subsequently the cartilage and hydrogel were compressed for 5 min at 10 mN force. The tensile force, applied at 100 mN min^{-1}, was measured to determine the adhesion strength at the interface between the cartilage and the hydrogel. Two other tests were conducted, one on a mineralized sample of the hydrogel without any binding peptide attached to a piece of

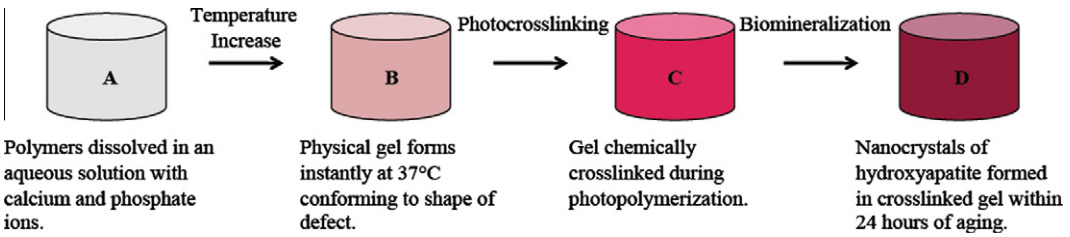

Fig. 2. Schematic depiction of the synthesis procedure for the fully mineralized hydrogel. It progresses to cartilage-like material properties once it is fully mineralized.

cartilage, the other on HBP-containing hydrogel without mineralization.

2.3.4. Statistical analysis

To determine whether the different data sets were significant, a two-tailed *t*-test was used with an α value of 0.1 and $n - 1$ degrees of freedom with $n = 5$ as the sample size.

3. Results

3.1. Nanocomposite characterization

TGA results obtained by heating the material to 700 °C showed a 15 wt.% inorganic content in the gels. Analysis in BF TEM mode revealed well-formed rounded nanoparticles of the inorganic phase with a mean particle size of approximately 40 nm (Fig. 3). XRD results (not shown) confirmed that the inorganic phase was brushite, a form of calcium phosphate.

3.2. Compression testing

Compression testing of the mineralized material demonstrated compressive moduli of similar magnitude to bovine cartilage (Fig. 4). The mineralized material compressive modulus was 0.64 ± 0.1 MPa, compared with 0.35 ± 0.1 MPa for bovine cartilage. Statistically, the difference in the average strain values was significant at or below 7% strain. In a series of tests (not shown) varying the photopolymerizing energy from 25 to 250 mW cm^{-2} and exposure time from 30 to 300 s had little effect on the compressive modulus of five separate specimens. All specimens were slightly stiffer than bovine cartilage. The concentration of HBP can be altered to adjust the compressive strength.

3.3. Shear testing

Shear testing was conducted on isolated samples of the mineralized material with or without addition of CBP. Non-mineralized variations of the hydrogel samples that acted as controls provided critical information on the impact of mineralization and the contribution of CBP and HBP to the mechanical strength of the hydrogel materials. Non-mineralized samples containing only HBP were unable to withstand the loading force during rheological testing, nor bonded properly when interfaced with cartilage. In contrast, non-mineralized HBP/CBP-containing samples resisted shear loading, but did not effectively bond to bovine cartilage. All differences were found to be statistically significant at a *P* value of 0.1.

Mineralization significantly increased the shear strength of the material. Mineralized samples demonstrated slightly stiffer shear moduli compared with bovine cartilage (Fig. 5). However, gross deformation features of the mineralized samples and cartilage were very similar (Fig. 5). The shear modulus of bovine cartilage at 20% strain was approximately 0.7 GPa, compared with 1.5–2 GPa in the four experimental specimens. Addition of CBP did not affect the shear moduli of the mineralized material. Subsequently we tested a composite structure consisting of the mineralized material bonded to a piece of bovine cartilage. This test was conducted to determine how well the co-polymer bonded to cartilage. These tests demonstrated excellent bonding characteristics to cartilage with shear moduli again slightly stiffer than native cartilage, but with similar deformation characteristics (Fig. 5). Furthermore, shear deformation occurred uniformly through the material and cartilage and was not preferentially concentrated at the bonding interface between the material and cartilage. G^* response

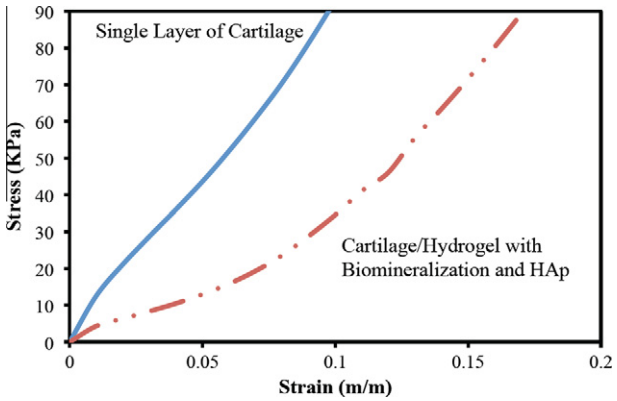

Fig. 4. Compressive stress–strain load deformation on an average of five samples for articular bovine cartilage and cartilage/hydrogel interface specimens. The single layer of articular cartilage (blue line) performed similarly to the hydrogel with HAp (orange dot dash line) and cartilage/hydrogel system with HAp (brown dots). No significant difference was seen on the addition of CBP with (green double line) and without (lilac triple line) the cartilage interface.

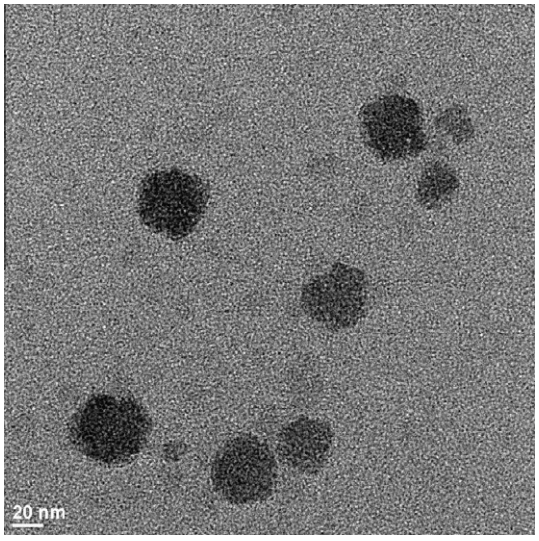

Fig. 3. Bright field transmission electron micrograph obtained at a magnification of 64,000×. The average particle size is approximately 40 nm.

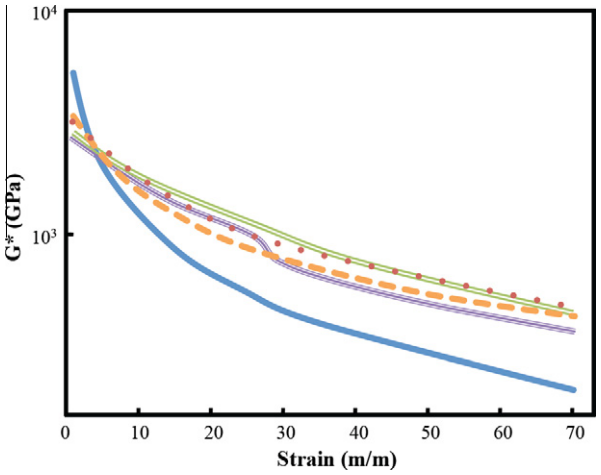

Fig. 5. Shear modulus of four mineralized samples and control bovine cartilage. The experimental samples are stiffer in shear strength than the cartilage (blue line). The HAp/CBP samples with (green double line) and without (lilac triple line) the cartilage interface are slightly stiffer than the HAp alone counterpart with (brown dots) and without (orange dot dash line) the cartilage interface.

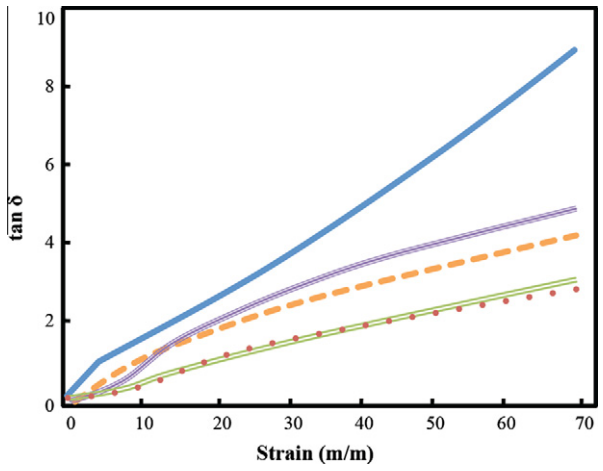

Fig. 6. Tan δ response of four mineralized experimental samples and bovine cartilage. The experimental samples have a smaller phase angle than the cartilage (blue line). The samples with HAp (orange dot dash line) and CBP (lilac triple line) without the cartilage interface have a larger loss to storage ratio than the corresponding HAp (brown dots) and CBP (green double line) samples with the interface.

curves for the hydrogel and cartilage samples bear more of a resemblance to that of G' than G''.

Tan δ responses (Fig. 6) for cartilage and mineralized experimental samples were directly proportional to strain magnitude. Increases in tan δ (the ratio of viscous deformation/elastic deformation in a viscoelastic material) indicate a material is becoming more viscous with increased deformation. As strain increased the mineralized hydrogel remained more elastic than native cartilage. Furthermore, the composite samples of the mineralized material bonded to cartilage were particularly resistant to increasing viscous behavior at higher strains (Fig. 6).

3.4. Tensile testing

The tensile modulus of bovine cartilage was 0.9 ± 0.1 MPa, compared with 0.5 ± 0.1 MPa for bovine cartilage bonded to the mineralized material loaded with HBP and 0.4 ± 0.05 MPa for bovine cartilage bonded to the mineralized material with carboxyl end groups (Fig. 7). These measured values are statistically significant at a P value of 0.05. In contrast, there was no adhesion between the non-mineralized material with HBP and the cartilage sample

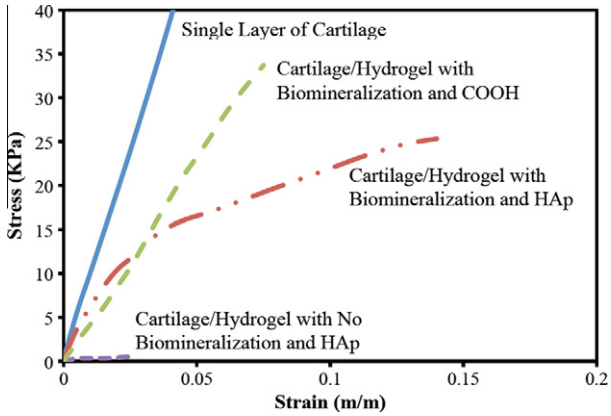

Fig. 7. Average tensile strength of four samples of the mineralized hydrogel with HAp bonded to cartilage, mineralized hydrogel with carboxyl end groups bonded to cartilage, and unmineralized hydrogel with HAp bonded to cartilage compared with bovine cartilage.

in tensile testing, giving it a modulus of <0.01 MPa. Overall, the bonded samples with mineralization were slightly weaker in tension but demonstrated good bonding strength. The samples without mineralization and specimens without CBP bonded to cartilage (data not shown) developed minimal tensile strength in tension testing.

4. Discussion

Paramount in understanding the pathomechanisms leading to PTOA is to decipher how localized AMD temporally and spatially propagates into widespread PTOA. Intact cartilage harbors a structural/metabolic reciprocal relationship between the interstitium of the cartilage and embedded chondrocytes. The cartilage interstitium converts a variety of external loads into physiologically healthy strains that are transmitted to the chondrocytes [26]. In turn, the chondrocytes transduce the favorable physiological strains and produce appropriate matrix molecules to support the cartilage interstitium. AMD disrupts this reciprocal relationship. Local damage disrupts the cartilage structure, chondrocytes are injured, rendering many cells physiologically incompetent, and many chondrocytes die [10,15,27,28]. Structural damage to the cartilage leads to a mechanically incompetent tissue that can no longer transmit healthy strain to the chondrocytes. Abnormal tissue strains are exacerbated by injury-related cartilage swelling and decreased osmolarity in regions of AMD [26,29].

The material synthesized in this investigation is a novel development for the treatment of AMD sustained by cartilage. To the best of our knowledge this is the first material specifically developed to treat both the mechanical and biological pathophysiological components of AMD. The material has not been developed to serve as a long-term cartilage replacement, which many others have tried to develop (reviewed by Hettrich et al. [30]) (there are 637 citations in PubMed returned for the search combination "cartilage defect" and "cartilage regeneration"). Rather, this material is designed to exert its mechanical and biological functions and subsequently mechanically disintegrate into small (<12.6 kDa) nontoxic constituents.

The physical premise for developing this material is to prevent impact injured chondrocytes from exposure to abnormal cartilage tissue deformation and swelling after an injury during the acute and subacute time periods. Several investigators have shown that healthy chondrocytes subjected to abnormal strain become metabolically dysfunctional or die [14,16,18]. Others have shown that healthy chondrocytes exposed to abnormal tissue swelling in the surrounding ground substance are also metabolically dysfunctional and at risk of chondrocyte death [27,29]. It stands to reason that impact injured chondrocytes would be affected more than healthy chondrocytes under similar adverse mechanical conditions. Chondrocytes in proximity to AMD after injury would be subjected to both abnormal tissue strains due to local disruption of the cartilage matrix and local cartilage swelling. We have hypothesized that restoring normal tissue mechanical behavior in the proximity of injured chondrocytes at the time of injury will increase the number of chondrocytes that survive and resume normal metabolic function. Cartilage impact studies have shown that chondrocytes die within hours by necrosis, followed by a wave of cell death by apoptosis over the next 1–2 weeks. The co-polymer has been developed to remain securely bonded to injured cartilage for the duration of this subacute time period.

Clinical outcome data clearly demonstrate that there is a need for a change in treatment strategy for intra-articular fractures (Fig. 1). AMD sustained by cartilage is an obvious target for intervention. Multiple investigations have demonstrated that chondrocytes in impacted cartilage become metabolically dysfunctional or

die [6,7,9,13,14,16,31]. Furthermore, the majority of impact-associated chondrocyte death and dysfunction consistently occurs in the regions sustaining the greatest injury adjacent to fracture lines and cartilage matrix cracks [15,21,32].

While chondrocyte death concentrates around overt matrix damage initially, it has been shown that both chondrocyte death and metabolic dysfunction propagate spatially and temporally after an injury [7,9,13,18]. Several investigators have demonstrated that apoptotic chondrocyte death occurred for at least 7 days post-injury [9,32]. Investigators have also shown that chondrocyte death and dysfunction expand outwardly from the zone of injury into the surrounding cartilage [7,9,13]. In summary, impact-related chondrocyte death and dysfunction have been clearly shown to concentrate in regions of AMD, and chondrocyte death and dysfunction are active processes that propagate after injury has occurred. Taken together, a therapeutic target exists to prevent propagation of AMD to PTOA by treating cartilage sustaining AMD.

The co-polymer developed in this experiment has favorable physical properties that allow its use to treat AMD sustained by cartilage. The co-polymer exists as a liquid at room temperature, but will form a hydrogel at body temperature. This will allow it to be injected into an injured joint as a liquid and infiltrate deep into matrix cracks and fracture edges in regions of AMD. Subsequently the co-polymer will physically transition to a gel while binding to cartilage in matrix cracks and in fracture lines through mineralization, allowing the material to remain securely bonded to injured cartilage surfaces in regions of AMD. Finally, the co-polymer can be photopolymerized, creating a local composite material that helps to restore native material properties to damaged cartilage.

In this paper we have demonstrated the development of a material that has compressive and shear stiffness comparable with bovine cartilage. The shear and compressive moduli were slightly higher than those of cartilage, but these properties can be modulated by modifying the constituent compositions and inorganic content. The co-polymer formed secure bonds with cartilage, which was demonstrated by shear testing composite samples of the mineralized co-polymer bonded to bovine cartilage (Figs. 5 and 6). These findings were confirmed by performing direct tensile testing of the mineralized samples bonded to bovine cartilage (Fig. 7). The tensile modulus of bovine cartilage was 1.0 MPa, compared with 0.5 MPa for bovine cartilage bonded to the mineralized material with HBP or carboxyl end groups (Fig. 7). In contrast, there was no adhesion between the non-mineralized material with HBP and the cartilage sample in tensile testing. This shows that in situ mineralization is essential for the implant to form a good interface with cartilage. Secure bonding between the co-polymer and surrounding cartilage will likely be important in clinical applications, which will allow the co-polymer to resist pathological tensile and shear strains in regions of AMD, and also allow the co-polymer to resist pathological localized strains resulting from injury-related swelling of the cartilage.

While the co-polymer has been developed to act as a mechanical stabilizing material, it can also serve as a carrier of chondrocyte-enhancing bioagents. Multiple investigations have demonstrated that multiple bioactive agents prevent chondrocyte death and improve chondrocyte biosynthetic function after an injury [9,13,32,33]. In the future the co-polymer could be loaded with a variety of agents that can be delivered directly to the most injured and damaged regions.

5. Conclusions

A novel nanocomposite photopolymerized hydrogel has been developed that will be capable of infiltrating damaged cartilage and potentially restoring native mechanical properties to local damaged tissue after an injury, based on in vitro tensile, compressive and shear moduli measurements. In situ mineralization with calcium phosphate nanocrystals significantly enhances the mechanical strength of the hydrogels. The nanocrystals reinforce the structure of the gels, allowing them to withstand greater forces and deformation. Furthermore, the mineralized co-polymer securely adheres to the surrounding cartilage, which will restore tensile and shear resistance to loading in damaged regions. It is hypothesized that mechanical restoration of damaged cartilage can potentially prevent propagation of chondrocyte dysfunction and death after an injury, which will prevent PTOA.

Acknowledgements

We would like to acknowledge Colin Paul who assisted with a lot of the initial work on this project through NSF-REU Grant EEC 0851519. We would like to acknowledge financial support from the Department of Energy's Science Undergraduate Laboratory Internship (DOE-SULI) program that supported Trishelle Copeland-Johnson. Support from the University of Iowa Vice Provost's office and NIH CORT grant on Post-Traumatic Osteo-Arthritis is gratefully acknowledged.

Appendix A. Figures with essential color discrimination

Certain figures in this article, particularly Figs. 1, 2 and 4–7, are difficult to interpret in black and white. The full color images can be found in the on-line version, at doi:10.1016/j.actbio.2011.04.010.

References

[1] Honkonen SE. Degenerative arthritis after tibial plateau fractures. J Orthop Trauma 1995;9(4):273–7.
[2] Marsh JL, Weigel DP, Dirschl DR. Tibial plafond fractures. How do these ankles function over time? J Bone Joint Surg Am 2003;85A(2):287–95.
[3] Matta JM. Fractures of the acetabulum: accuracy of reduction and clinical results in patients managed operatively within three weeks after the injury. J Bone Joint Surg Am 1996;78(11):1632–45.
[4] Ovadia DN, Beals RK. Fractures of the tibial plafond. J Bone Joint Surg Am 1986;68(4):543–51.
[5] Volpin G, Dowd GS, Stein H, Bentley G. Degenerative arthritis after intra-articular fractures of the knee. Long-term results. J Bone Joint Surg Br 1990;72(4):634–8.
[6] Borrelli Jr J, Silva MJ, Zaegel MA, Franz C, Sandell LJ. Single high-energy impact load causes posttraumatic OA in young rabbits via a decrease in cellular metabolism. J Orthop Res 2009;27(3):347–52.
[7] Clements KM, Burton-Wurster N, Lust G. The spread of cell death from impact damaged cartilage: lack of evidence for the role of nitric oxide and caspases. Osteoarthritis Cartilage 2004;12(7):577–85.
[8] Duda GN, Eilers M, Loh L, Hoffman JE, Kaab M, Schaser K. Chondrocyte death precedes structural damage in blunt impact trauma. Clin Orthop Relat Res 2001;393:302–9.
[9] Hurtig M, Chubinskaya S, Dickey J, Rueger D. BMP-7 protects against progression of cartilage degeneration after impact injury. J Orthop Res 2009;27(5):602–11.
[10] Krueger JA, Thisse P, Ewers BJ, Dvoracek-Driksna D, Orth MW, Haut RC. The extent and distribution of cell death and matrix damage in impacted chondral explants varies with the presence of underlying bone. J Biomech Eng 2003;125(1):114–9.
[11] Mankin HJ. The reaction of articular cartilage to injury and osteoarthritis. N Engl J Med 1974;291(24):1285–92.
[12] Pascual Garrido C, Hakimiyan AA, Rappoport L, Oegema TR, Wimmer MA, Chubinskaya S. Anti-apoptotic treatments prevent cartilage degradation after acute trauma to human ankle cartilage. Osteoarthritis Cartilage 2009;17(9):1244–51.
[13] Baars DC, Rundell SA, Haut RC. Treatment with the non-ionic surfactant poloxamer P188 reduces DNA fragmentation in cells from bovine chondral explants exposed to injurious unconfined compression. Biomech Model Mechanobiol 2006;5(2/3):133–9.
[14] Chen CT, Burton-Wurster N, Borden C, Hueffer K, Bloom SE, Lust G. Chondrocyte necrosis and apoptosis in impact damaged articular cartilage. J Orthop Res 2001;19(4):703–11.
[15] Lewis JL, Deloria LB, Oyen-Tiesma M, Thompson Jr RC, Ericson M, Oegema Jr TR. Cell death after cartilage impact occurs around matrix cracks. J Orthop Res 2003;21(5):881–7.

[16] Chen CT, Burton-Wurster N, Lust G, Bank RA, Tekkopele JM. Compositional and metabolic changes in damaged cartilage are peak-stress, stress rate and loading-duration dependent. J Orthop Res 1999;17(6):870–9.
[17] Jeffrey JE, Aspden RM. The biophysical effects of a single impact load on human and bovine articular cartilage. Proc Inst Mech Eng [H] 2006;220(6):677–86.
[18] Morel V, Quinn TM. Short-term changes in cell and matrix damage following mechanical injury of articular cartilage explants and modelling of microphysical mediators. Biorheology 2004;41(3/4):509–19.
[19] Barei DP, Nork SE, Mills WJ, Coles CP, Henley MB, Benirschke SK. Functional outcomes of severe bicondylar tibial plateau fractures treated with dual incisions and medial and lateral plates. J Bone Joint Surg Am 2006;88(8):1713–21.
[20] Olson SA, Bay BK, Chapman MW, Sharkey NA. Biomechanical consequences of fracture and repair of the posterior wall of the acetabulum. J Bone Joint Surg Am 1995;77(8):1184–92.
[21] Enlow D, Rawal A, Kanapathipillai M, Schmidt-Rohr K, Mallapragada S, Lo CT, et al. Synthesis and characterization of self-assembled block copolymer templated calcium phosphate nanocomposite gels. J Mater Chem 2007;17:1570–8.
[22] Kanapathipillai M, Yusufoglu Y, Rawal A, Hu YY, Lo CT, Thiyaigarajan P, et al. Synthesis and characterization of ionic block copolymer templated calcium phosphate nanocomposites. Chem Mater 2008;20:5922–32.
[23] Yusufoglu Y, Hu Y, Kanapathipillai M, Kramer M, Kalay YE, Thiyagarajan P, et al. Bioinspired synthesis of self-assembled calcium phosphate nanocomposites using block copolymer-peptide conjugates. J Mater Res 2008;23:3196–212.
[24] Bali D, King L, Kim S. Synthesis of new gramicidin A derivatives. Aust J Chem 2003;56:293.
[25] Zeng F, Lee H, Allen C. Epidermal growth factor conjugated poly(ethylene glycol)-block-poly(d-valerolactone) copolymer micelles for targeted delivery of chemotherapeutics. Bioconjug Chem 2006;17:399.
[26] Guilak F, Jones WR, Ting-Beall HP, Lee GM. The deformation behavior and mechanical properties of chondrocytes in articular cartilage. Osteoarthritis Cartilage 1999;7(1):59–70.
[27] Bush PG, Hodkinson PD, Hamilton GL, Hall AC. Viability and volume of in situ bovine articular chondrocytes – changes following a single impact and effects of medium osmolarity. Osteoarthritis Cartilage 2005;13(1):54–65.
[28] Milentijevic D, Helfet DL, Torzilli PA. Influence of stress magnitude on water loss and chondrocyte viability in impacted articular cartilage. J Biomech Eng 2003;125(5):594–601.
[29] Narmoneva DA, Wang JY, Setton LA. Nonuniform swelling-induced residual strains in articular cartilage. J Biomech 1999;32(4):401–8.
[30] Hettrich CM, Crawford D, Rodeo SA. Cartilage repair: third-generation cell-based technologies – basic science, surgical techniques, clinical outcomes. Sporta Med Arthrosc 2008;16(4):230–5.
[31] Green DM, Noble PC, Ahuero JS, Birdsall HH. Cellular events leading to chondrocyte death after cartilage impact injury. Arthritis Rheum 2006;54(5):1509–17.
[32] D'Lima DD, Hashimoto S, Chen PC, Colwell Jr CW, Lotz MK. Human chondrocyte apoptosis in response to mechanical injury. Osteoarthritis Cartilage 2001;9(8):712–9.
[33] Martin JA, McCabe D, Walter M, Buckwalter JA, McKinley TO. *N* -Acetylcysteine inhibits post-impact chondrocyte death in osteochondral explants. J Bone Joint Surg Am 2009;91A:1890–7.